

Recognizing the constitution of small bodies in extreme-mass-ratio inspirals by gravitational waves

Shu-Cheng Yang,¹ Run-Dong Tang,^{1,2} Xing-Yu Zhong,^{1,2} Yuan-Hao Zhang,^{3,2} and Wen-Biao Han^{3,1,2,4,*}

¹*Shanghai Astronomical Observatory, Chinese Academy of Sciences, Shanghai 200030, China*

²*School of Astronomy and Space Science, University of Chinese Academy of Sciences, Beijing 100049, China*

³*Hangzhou Institute for Advanced Study, University of Chinese Academy of Sciences, Hangzhou 310124, China*

⁴*Shanghai Frontiers Science Center for Gravitational Wave Detection, 800 Dongchuan Road, Shanghai 200240, China*

(Dated: September 5, 2022)

The extreme mass ratio inspirals (EMRIs) are promising gravitational wave (GW) sources for space-borne GW detectors. The signals of EMRIs usually have long timescales, ranging from several months to several years, and their detection requires accurate GW signal templates. In most waveform models, the compact objects in EMRIs are considered test particles, which do not consider the small bodies' spin, mass distribution, and tidal deformation. In this work, we simulate the GW signals of EMRIs by considering the compact objects' spin and mass quadrupole. We find that a compact object's spin can significantly influence the GW signals, and the tidal-induced and spin-induced quadrupoles matter only if the compact objects are white dwarfs, especially EMRIs of a higher symmetric mass ratio. We can distinguish white dwarfs from other compact objects in this case. The structures of black holes and neutron stars in EMRIs do not have detectable effects on GW signals. Furthermore, compared with the GW signals that use test particle approximation, the signal-to-noise ratios (SNRs) of GW signals that consider extended bodies decrease slightly, which hints that we can omit the spin and quadrupole of the compact object in the detection of EMRIs.

PACS numbers: 04.70.Bw, 04.80.Nn, 95.10.Fh

I. INTRODUCTION

The properties of compact objects, such as black holes, neutron stars, and white dwarfs, are profound in astrophysics and gravitational physics. The observations of GWs from compact binary coalescences since 2015 ushered in a new era for solving the above problems using GWs [1, 2]. There are abundant sources that emit GWs in the low-frequency band, which can be observed by future space-borne GW detectors [3]. EMRIs, which consist of central massive black holes (MBHs) and orbiting small compact objects, are essential GW sources for space-borne GW detectors [3, 4]. The small object in an EMRI could be a stellar-mass black hole, neutron star, white dwarf, and other compact objects. EMRIs emit GWs when the small objects orbit the central MBHs. In this sense, the dynamical behavior of such compact objects is critical for low-frequency GW astronomy.

Nowadays, the spin interaction of relativistic systems has become an important subject. For this reason, it is a real concern to properly understand the dynamics of extended bodies in curved space-time that includes classical spin. The dynamic is simple when one considers the point-particle approximation. Nevertheless, once considering the structure, the problem is hard to solve. In Newtonian mechanics, a solution to the problem of the motion of N isolated bodies with internal structure was first proposed by F. Tisserand [5]. In his work, Tisserand was able to separate the body's external and internal motion by considering the equations' linearity. In this way, it was possible to describe the dynamics of one of the bodies with high precision. However, in contrast to Newtonian gravity, the field equations of general relativity are coupled and nonlinear. Therefore, it is not possible to apply the same methods of Newtonian mechanics. In general relativity, it is well-known that a point-particle follows a geodesic. However, if we consider extended bodies, it is necessary to consider the body's effect in the space-time metric, an effect known as self-field [6].

The first approach to the problem of extended bodies in general relativity was in 1937 with the work of M. Mathisson [7], who demonstrated an existing interaction between the Riemann curvature tensor and the moving particle's spin in the equations of motion. Mathison showed that it is possible to define force, center-of-mass, torque, and mass in a relativistic theory. The problem of extended bodies in general relativity also was considered by Papapetrou [8–10], where he uses a similar approach. Latter, B. Tulczyjew, and W. Tulczyjew improved and developed the methods of Mathison [11, 12]. On the other hand, improvements on the definition of the center-of-mass were

* corresponding author: wbhan@shao.ac.cn

made by Moller and others in Refs. [13–18]. Today, the equations that describe the motion of extended bodies with spin and mass are known as the Mathison-Papapetrou-Dixon equations (MPD).

When considering the inspiral orbital motion of an equal-mass spinning binary system, it is crucial to consider the higher-order multipole moment contributions [19]. Nevertheless, in the case of EMRIs, it makes sense to truncate the multipole expansion and focus mainly on the pole-dipole approximation. In general, calculations involving spinning objects with dimensions sufficiently small compared to the background space-time’s local curvature radius can be performed with good approximation by employing the MPD equations of motion. In the literature, there are a variety of astrophysical situations where the MPD equations are used to show the impact of spin-curvature interactions between spinning particles and black holes [20–23]. From the numerical point of view, it is possible to investigate the limits of stability for the MPD equations [23–26]. In the work of S. Suzuki and K. Maeda [23], the authors studied the stability of circular orbits for spinning test particles in Kerr space-time. They showed that orbits in the radial direction are stable, while some circular orbits become unstable in the direction perpendicular to the equatorial plane. Moreover, in the case of particles with higher spin, the innermost stable circular orbit (ISCO) appears before the minimum of the effective potential in the equatorial plane disappears.

Using the MPD equation, it is possible to derive predictions of gravitational wave generation expected to occur from spin-induced deviations away from geodesic motion. In Ref. [27], Yasushi Mino et al. used Teukolsky, Sasaki, and Nakamura’s formalisms to perturb the Kerr black hole and calculate the energy flux and the waveform induced by a spinning particle falling from infinity into a rotating black hole. Due to the combination of Teukolsky formalism with the MPD equations, the authors found two additional effects related to the particles’ spin: the first effect is due to the spin-spin interaction force, and the other is due to the contribution of the energy-momentum tensor of the spinning particle. According to the numerical calculations, the authors argue that these effects are significant. In this sense, a deeper understanding of the relativistic two-body problem requires accurate and general results from both numerical and analytic computations.

In this article, we use the MPD equation to simulate the GW signals of EMRIs that consider the compact objects’ spin and quadrupole to study to what extent these parameters could influence the GW signals. We find that, for the GW signals of EMRI, the spin of compact objects is influential. The tidal-induced and spin-induced quadrupoles have no influence only if the compact objects are white dwarfs, especially EMRIs of higher symmetric mass ratio. Therefore, we may distinguish white dwarfs from other compact objects. Moreover, the SNRs of GW signals that consider extended bodies decrease slightly compared with the GW signals that use test particles. Therefore, in the detection of EMRIs, we may omit the spin and quadrupole of the compact object in constructing the waveform templates of EMRIs.

This paper is organized as follows, Sec. II starts with the equation of motion for extended bodies. Then we introduce the gravitational waves of EMRIs In Sec. III. In Sec. IV, we present our results in detail. Finally, we draw the conclusion in Sec. V. Through this paper, we use Einstein summation convention.

II. CHARACTERISTICS OF SMALL BODIES IN EMRIS

The accuracy of the waveform templates is crucial in GW detection. Therefore, we need to work out accurate orbits of small bodies. The MPD equations describe the motion of extended bodies in curved space-time with spin and mass multipole moments. The higher-order terms of the MPD equations (expanded by multipole moments) show that the inner structure of small bodies slightly influences the orbit[28]. In this article, we considered the EMRI model that uses extended bodies with spin and quadrupole moments, which fit the actual orbits better than the models that use test particles. In this case, the motion equations of the small bodies are (using natural units of $G = c = 1$)[16]

$$\dot{p}^\mu = -\frac{1}{2}S^{\alpha\beta}v^\rho R^\mu_{\rho\alpha\beta} - F^\mu, \quad (2.1)$$

$$\dot{S}^{\alpha\beta} = 2p^{[\alpha}v^{\beta]} + G^{\alpha\beta}, \quad (2.2)$$

where p^μ is the four-momentum of small compact bodies, defined as $p^\mu = mu^\mu$, and m is defined as the dynamical mass of compact bodies, satisfying the condition $m^2 = -p^\mu p_\mu$, it depends on four-momentum of compact bodies, so m is not a constant. The dot above means the differential with respect to proper time τ of momentum vector and spin tensor respectively[18]. u^μ is the dynamical velocity of bodies, satisfying the condition $u^\mu u_\mu = -1$. $S^{\alpha\beta}$ is a second-order anti-symmetrical spin tensor, which satisfies the spin conservation condition $S^2 = S^\mu S_\mu = \frac{1}{2}S^{\mu\nu}S_{\mu\nu}$. $v^\rho = dz^\rho/d\tau$ is the kinematical four-velocity of extended bodies, $z(\tau)$ is the world line of the extended bodies’ mass center, which is determined by the supplementary condition $u_\lambda S^{\kappa\lambda} = 0$. $R^\mu_{\rho\alpha\beta}$ is the Riemannian curvature tensor,

F^μ and $G^{\alpha\beta}$ is the coupling terms between the quadrupole and background gravitational field:

$$F^\mu = \frac{1}{6} J^{\alpha\beta\gamma\sigma} \nabla^\mu R_{\alpha\beta\gamma\sigma}, \quad (2.3)$$

$$G^{\alpha\beta} = \frac{4}{3} J^{\gamma\delta\epsilon[\alpha} R^{\beta]}_{\delta\epsilon\gamma}, \quad (2.4)$$

where $J^{\gamma\delta\epsilon\sigma}$ is the mass quadrupole tensor that has the same symmetry as $R_{\alpha\beta\gamma\sigma}$. The relationship between four-velocity and four-momentum is [29]

$$m^2 v^\sigma = m p^\sigma - F^{\sigma\rho} p_\rho + \frac{2m p^\rho R_{\mu\rho\alpha\beta} S^{\sigma\mu} S^{\alpha\beta} - 2p_\delta F^{\rho\delta} R_{\mu\rho\alpha\beta} S^{\sigma\mu} S^{\alpha\beta} + 4m^2 F_\mu S^{\sigma\mu}}{4m^2 + R_{\mu\rho\alpha\beta} S^{\sigma\mu} S^{\alpha\beta}}. \quad (2.5)$$

When $v^\mu v_\mu = -1$, τ is the proper time. Generally speaking, the kinematical mass $\bar{m} = p^\mu v_\mu$ is not equals to the dynamical mass m , but in this article we use orthogonal condition $u^\mu v_\mu = -1$, where $m = \bar{m}$.

The mass quadrupole tensor takes the form[30]:

$$J^{\alpha\beta\gamma\delta} = \frac{3m}{\bar{m}^3} p^{[\alpha} Q^{\beta][\gamma} p^{\delta]}, \quad (2.6)$$

where the quadrupole of extended bodies

$$Q^{\alpha\beta} = C_Q S_\lambda^\alpha S^{\beta\lambda} + \frac{1}{\bar{m}^2} \mu_2 R^{\alpha\beta\gamma\delta} u_\gamma u_\delta, \quad (2.7)$$

C_Q is a dimensionless constant to measure the spin-induced quadrupole and is related to the equation of state (EOS) of extended bodies. Providing the radius and mass of a rotating compact body, C_Q can be approximately expressed by the equation[31]:

$$C_Q \approx -\frac{25}{8} \frac{Rc^2}{Gm}, \quad (2.8)$$

where G is the gravitational constant, c is the speed of light in vacuum, and R is the body's radius. C_Q varies for different compact bodies. For black holes, $|C_Q| = 1$; for neutron stars, $|C_Q|$ varies from 2 to 20 in different EOS[32–34]; for white dwarfs, $|C_Q|$ takes about 10^4 [35]. μ_2 represents the quadrupole produced by the tidal effect, and it takes the form[30]

$$\mu_2 = \frac{2k_2}{3} (R/\frac{Gm}{c^2})^5 \nu^4, \quad (2.9)$$

where k_2 is a dimensionless tidal love parameter determined by the EOS of compact bodies. ν is the symmetric mass ratio of EMRI ($\nu = mM/(m+M)^2$). Binnington and Poisson [36] proposed a relativistic tidal parameter theory that is applicable to compact bodies with strong inner gravity, for black holes $k_2 = 0$; for neutron stars $k_2 \sim 0.1$; for white dwarfs $k_2 \sim 0.01$ [37]. According to Eqn. 2.9, for black holes, $\mu_2 = 0$; for neutron stars with radius of 10 – 20 km, and mass of $1 - 2M_\odot$, μ_2/ν^4 is $\sim 10^2$ to $\sim 10^3$. for white dwarfs, as show in Table I, we calculate some values of C_Q and μ_2/ν^4 of white dwarfs .

s is the spin angular momentum of the small body in the EMRI. For a stellar black hole, the maximum spin angular momentum $s = m^2$ (using natural units of $G = c = 1$). However, for primordial black holes, $s \approx 0$ [38]. Neutron stars and white dwarfs can have spin magnitudes a little larger than m^2 . For convenience, we use dimensionless $\hat{s} = s/m^2$ in the following parts of this article. As shown in Table II, we summarize several physical characteristics for the small compact body in EMRI[39], such as stellar origin black holes(SOBHs), primordial black holes(PBHs), neutron stars(NSs) and white dwarfs(WDs).

When setting the orbit configuration and calculating the orbits of EMRIs, we consider the innermost stable circular orbit (ISCO) and tidal radius as the restrictions. ISCO is the smallest stable orbit for a test particle orbiting a massive object. For a rotating BH, the radius of ISCO is

$$R_{\text{ISCO}} = M[3 + Z_2 \pm \sqrt{(3 - Z_1)(3 + Z_1 + 2Z_2)}], \quad (2.10)$$

where

$$Z_1 = 1 + (1 - a^2)^{1/3} [(1 + a)^{1/3} + (1 - a)^{1/3}], \quad (2.11)$$

TABLE I. C_Q and μ_2/ν^4 of white dwarfs in different mass and radius

Mass(M_\odot)	Radius(R_\odot)	$ C_Q $	μ_2/ν^4
0.75	0.009	17668	3.85×10^{16}
1.003	0.0084	12330	6.38×10^{15}
1.1	0.0031	4149	2.75×10^{13}
1.2	0.0055	6748	3.13×10^{14}
1.28	0.0041	4716	5.22×10^{13}
1.3	0.004	4530	4.27×10^{13}
1.33	0.003	3321	9.04×10^{12}

TABLE II. Physical characteristics of compact objects.

	Mass(M_\odot)	\hat{s}	k_2	μ_2/ν^4	$ C_Q $
SOBH	$2 \sim 5 - 50 \sim 150$	$0 - 1$	0	0	1
PBH	$\sim 10^{-19} - \sim 10^3$	~ 0	0	0	1
NS	$1.1 - 2.1$	$\gtrsim 1.3$	~ 0.1	$\sim 10^2 - \sim 10^3$	$2 - 20$
WD	$0.2 - 1.44$	$\gtrsim 10$	~ 0.01	$\sim 10^{12} - \sim 10^{16}$	$\sim 10^3 - \sim 10^4$

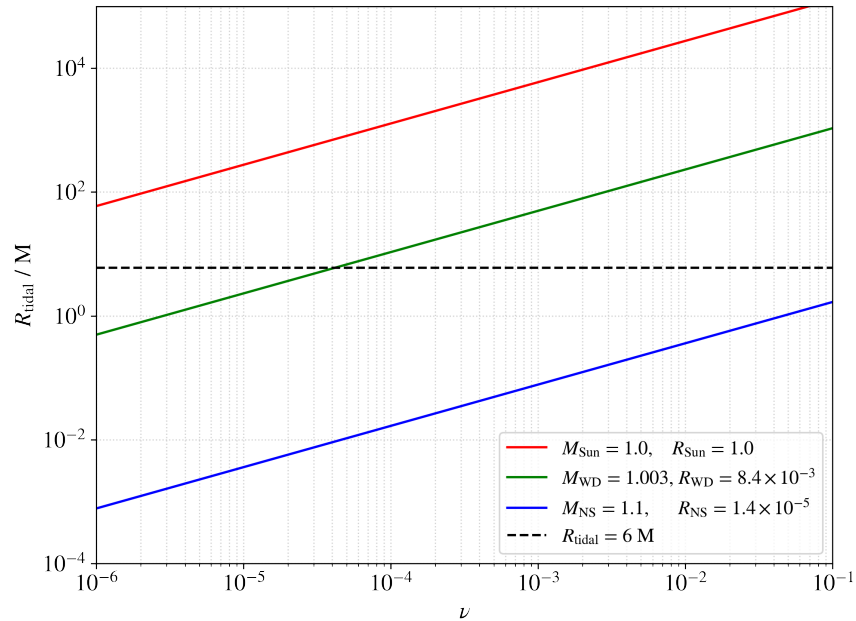


FIG. 1. The tidal radius R_{tidal} of EMRIs in different ν for different orbiting body. The red curve is for the Sun, the green curve is for a white dwarf, and the blue curve is for a neutron star. The black dotted curve marks $6 M$, which is the R_{ISCO} for a non-rotating black hole.

$$Z_2 = \sqrt{3a^2 + Z_1^2}. \quad (2.12)$$

with a as the rotation parameter of the rotating black hole. Eqn. (2.10) taking negative sign when the orbit is prograde, and taking positive sign when the orbit is retrograde. For an EMRI, inside the ISCO, no stable circular orbits exist. Another important concept is tidal radius [40]

$$R_{\text{tidal}} = 2^{1/3} \frac{R}{m} \nu^{2/3} M. \quad (2.13)$$

Inside the tidal radius, some compact stars such as white dwarfs and neutron stars would be torn apart by the tidal force of the central black hole. According to Eqn. (2.13), Fig 1 shows the tidal radius of EMRIs in different ν for

different orbiting body(the sun, a white dwarf and a neutron star). for an EMRI with $\nu = 10^{-6}$, the tidal radius for the sun is around 100 M, for white dwarf and neutron star are less than 1 M. for an EMRI with $\nu = 10^{-4}$, the tidal radius for the sun is 1278.88M, the tidal radius for white dwarf is 10.71M, the tidal radius for neutron star is 0.017M.

III. THE GRAVITATIONAL WAVES SIGNALS OF EMRIS

To work out the gravitational waves signals of EMRIs, we first calculate the geodesics. The geodesic equation without the radiation reaction effect is

$$\frac{du^\mu}{dt} = -\Gamma_{\rho\sigma}^\mu u^\rho u^\sigma, \quad (3.1)$$

$$u^\mu = \frac{dx^\mu}{dt}, \quad (3.2)$$

where x^μ is Boyer-Lindquist coordinate of the particle, u^μ is the 4-velocity and $\Gamma_{\rho\sigma}^\mu$ is Christoffel connection. Glampedakis, Hughes and Kennefick (GHK) [41] proposed a scheme for computing approximate generic EMRI trajectories. Providing the energy E , z-component of the angular momentum L^z , and Carter constant Q , the orbit of a small body in the EMRI will oscillate between periapsis r_p and apoapsis r_a ,

$$r_p = \frac{p}{1+e}, r_a = \frac{p}{1-e}, \quad (3.3)$$

then the semi-latus rectum p and eccentricity e can be calculated by [42]

$$p = \frac{2r_a r_p}{r_a + r_p}, e = \frac{r_a - r_p}{r_a + r_p}, \quad (3.4)$$

The orbital inclination angle ι can be calculated by

$$Q = L_z^2 \tan^2 \iota, \quad (3.5)$$

When considering the effect of radiation reaction, Eqn. (3.1) will be

$$\frac{du^\mu}{d\tau} = -\Gamma_{\rho\sigma}^\mu u^\rho u^\sigma + F^\mu, \quad (3.6)$$

where F is the radiation force, and can be recovered from the adiabatic radiation fluxes [43]

$$\dot{E}u^t = -g_{tt}F^t - g_{t\phi}F^\phi, \quad (3.7)$$

$$\dot{L}_z u^t = g_{t\phi}F^t + g_{\phi\phi}F^\phi, \quad (3.8)$$

$$\dot{Q}u^t = 2g_{\theta\theta}^2 u^\theta F^\theta + 2\cos^2\theta a^2 E\dot{E} + 2\cos^2\theta \frac{L_z \dot{L}_z}{\sin^2\theta}, \quad (3.9)$$

$$g_{\mu\nu}u^\mu F^\nu = 0, \quad (3.10)$$

$$F^r = -\frac{g_{\theta\theta}u^\theta F^\theta + g_{\phi\phi}u^\phi F^\phi + g_{tt}u^t F^t + g_{t\phi}u^t F^\phi + g_{\phi t}u^\phi F^t}{g_{rr}u^r}. \quad (3.11)$$

After getting the orbit, we calculate the gravitational waveform of EMRIs[44]

$$\bar{h}^{jk}(t, \mathbf{x}) = \frac{2}{r} \left[\dot{I}^{jk}(t') \right]_{t'=t-r} \quad (3.12)$$

$$I^{jk} = \mu x_p^j x_p^{jk} \quad (3.13)$$

where $\bar{h}^{\mu\nu} = h^{\mu\nu} - \frac{1}{2}\eta^{\mu\nu}\eta^{\rho\sigma}h_{\rho\sigma}$ is the trace-reversed metric perturbation [43]. We transform the waveform into transverse-traceless gauge and we get the plus and cross components of the waveform observed at latitudinal angle Θ and azimuthal angle Φ :

$$h_+ = h^{\Theta\Theta} - h^{\Phi\Phi} \quad (3.14)$$

$$= [\cos^2\Theta(h^{xx}\cos^2\Phi + h^{xy}\sin 2\Phi h^{yy}\sin^2\Phi) + h^{zz}\sin^2\Theta - \sin 2\Theta(h^{xz}\cos\Phi + h^{yz}\cos\Phi)]$$

$$- (h^{xx}\sin^2\Phi - h^{xy}\sin 2\Phi + h^{yy}\cos\Phi),$$

$$h_\times = 2h^{\Theta\Phi} \quad (3.15)$$

$$= 2[\cos\Theta(-\frac{1}{2}h^{xx}\sin 2\Phi + h^{xy}\cos 2\Phi + \frac{1}{2}h^{yy}\sin 2\Phi) + \sin\Theta(h^{xz}\sin\Phi - h^{yz}\cos\Phi)].$$

IV. DATA ANALYSIS AND RESULTS

As shown in Table II, the small compact object within the mass range $1 - 1.44 M_\odot$ could be primordial black holes, neutron stars, or white dwarfs. If we could get the spin or quadrupole moment information for the compact object in the EMRI, we may distinguish its constitution. For convenience, the mass of small compact objects is set to $1 M_\odot$ in the following calculations. Then we can focus on the spin and tidal effects and analyze if we can recognize the small objects with GWs signals from EMRIs.

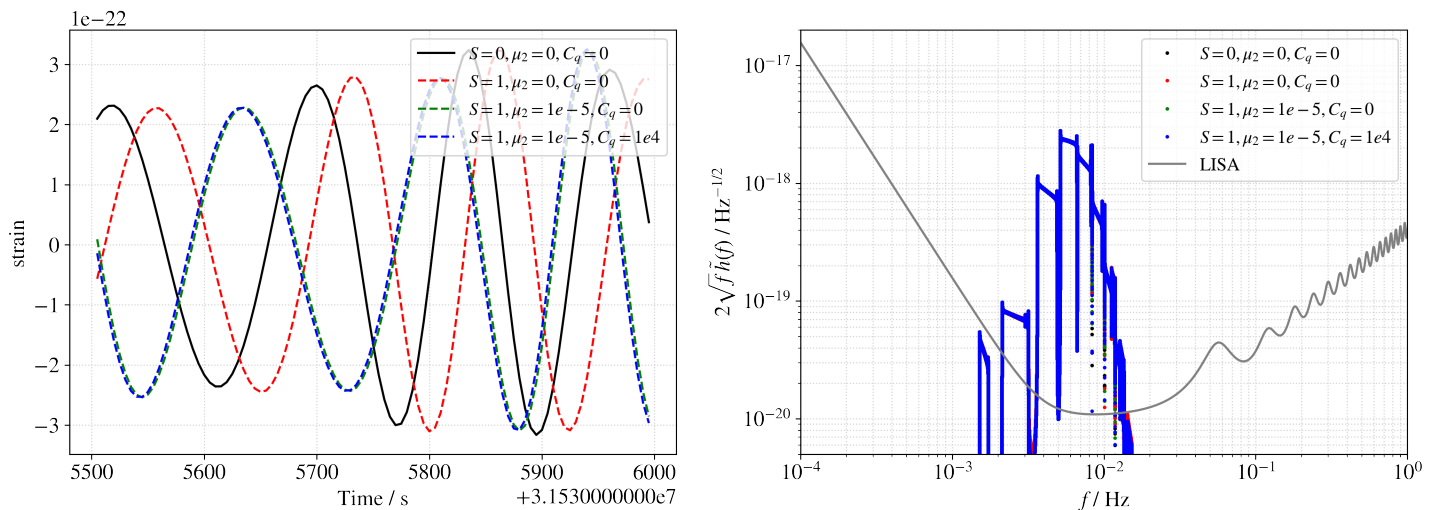


FIG. 2. The GW signals (h_+) of EMRIs in different configurations of \hat{s} , μ_2 and C_Q . The duration of signals is one year, $M_{\text{bh}} = 10^6 M_\odot$, $M_{\text{co}} = 1.0 M_\odot$, $a = 0.9$, $\iota_0 = 0.0$, $e = 0.2$ and $p = 5$. The left panel displays the GW signals in time domain, and the right panels displays them in frequency domain. In the frequency domain, the grey curve marks the sensitivity curve of LISA

In Fig. 2, we plot GW signals (h_+) of different EMRI configurations in the time domain (left panel) and frequency domain (right panel). In the frequency domain, the grey curve marks the sensitivity curve of space GW detector – LISA (Laser Interferometer Space Antenna). We show the influence on waveform phase by spin \hat{s} , tidal-induced quadrupole μ_2 , and spin-induced quadrupole C_Q of compact bodies. The duration of signals is one year, the mass of central black hole $M_{\text{bh}} = 10^6 M_\odot$, the mass of compact object $M_{\text{co}} = 1.0 M_\odot$, the Kerr parameter $a = 0.9$, the inclination angle of orbit $\iota_0 = 0.0$, the eccentricity $e = 0.2$, the semi latus rectum $p = 5$. The black curve is the initial GW signal without the influence of \hat{s} , μ_2 , and C_Q . The influence of \hat{s} , μ_2 , and C_Q are added successively in the red, green, and blue curves.

In the frequency domain of Fig. 2, the GW signals almost overlap, suggesting their SNRs are almost the same. We

need to calculate the SNRs of GW signals to ensure that. The SNR of the signals can be defined as [45]

$$\rho := \sqrt{\langle h|h \rangle}, \quad (4.1)$$

where $\langle h|h \rangle$ is the inner product of signal $h(t)$ itself. The inner product between signal $a(t)$ and template $b(t)$ is

$$\langle a|b \rangle = 2 \int_0^\infty \frac{\tilde{a}^*(f)\tilde{b}(f) + \tilde{a}(f)\tilde{b}^*(f)}{S_n(f)} df, \quad (4.2)$$

where $\tilde{a}(f)$ is the Fourier transform of $a(t)$, $\tilde{a}^*(f)$ is the complex conjugate of $\tilde{a}(f)$, and $S_n(f)$ is the power spectral density(PSD) of the GW detectors' noise. Throughout this paper, the PSD is taken to be the noise level of LISA. We first calculate the SNRs of several GW signals for EMRIs with $\hat{s} = 0$, $\mu_2 = 0$, and $C_Q = 0$, and then we calculate the SNRs of GW signals for EMRIs with different configurations of \hat{s} , μ_2 , and C_Q . Fig. 3 shows the relative difference between the former and latter signals' SNRs. We can see the influence of \hat{s} , μ_2 , and C_Q on the GW signal of EMRIs is about 10^{-4} to 10^{-6} , so we may say the spin and quadrupole of the compact object are not important in constructing the gravitational waveform models of EMRIs.

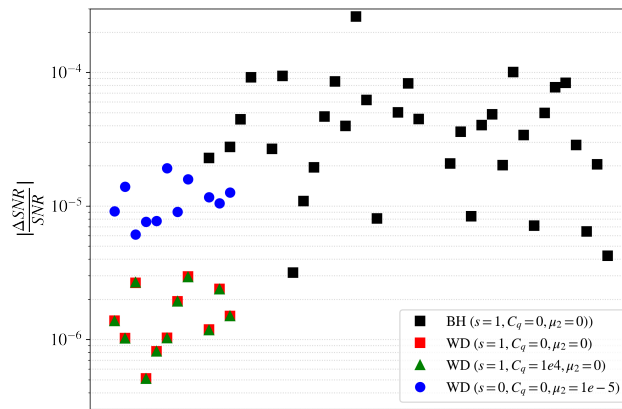


FIG. 3. The relative difference $\Delta \text{SNR} / \text{SNR}$ between EMRIs consider or not consider \hat{s} , μ_2 , and C_Q . The black squares marks the EMRIs with M_{co} of tens of solar mass. The red squares, green triangles, and blue circles marks the EMRIs with M_{co} of one solar mass around.

In the time domain of Fig. 2, during the last seconds of the orbit evolution, we can see the influence of \hat{s} and μ_2 is significant, while the influence of C_Q is tiny. For further discussion of the quantified difference between the GW signals and the templates, we adopt the well-known matched-filtering technology, we use maximized fitting factor(overlap)

$$\text{FF}(a, b) = \max_{t_s, \phi_s} \frac{\langle a(t)|b(t+t_s)e^{i\phi_s} \rangle}{\sqrt{\langle a|a \rangle \langle b|b \rangle}}, \quad (4.3)$$

where t_s is the time shift t_s and ϕ_s is the phase shift. We use overlap to quantify the differences between the GW signals and the templates, and the results of overlap is calculated by PyCBC[46].

The result of overlaps between the GW signals and templates are shown in Fig.4, Fig.5 and Fig.6. In this work, we set a criteria value of 0.97 for overlap as Ref. [47]. If the overlap value is greater than 0.97, then we say the difference between the GW signals and templates is insignificant, and we could use this template in searching for GW signals of this kind. Fig.4 show the overlaps between the GW templates ($\hat{s} = 0$) and the GW signals that changed with the compact body's spin \hat{s} . We can see that for all GW signals, the overlaps decrease when \hat{s} goes up. The overlaps down to 0.97 for most cases. Therefore, we could distinguish SOBH($\hat{s} = 0$) from compact objects with higher spin. Fig.5 show the overlaps between the GW templates ($\mu_2 = 0$) and the GW signals that changed with the compact body's tidal-induced quadrupole μ_2 . Fig.5 shows that the overlaps decrease when μ_2 goes up for all GW signals. However, for EMRIs of different ν , only μ_2 in the corresponding region is valid. There are only the μ_2 ranges of white dwarfs shown in Fig.5, and the μ_2 ranges of black holes and neutron stars are too small to be shown. For the $\nu = 10^{-6}$ case (red curve), the valid overlaps keep greater than 0.97, and we can not identify μ_2 of white dwarfs. For EMRIs with $\nu = 10^{-5}$ and $\nu = 10^{-4}$, especially $\nu = 10^{-4}$ case, it is possible to identify μ_2 of white dwarfs. Fig.6 show the overlaps between the GW templates ($C_Q = 0$) and the GW signals that changed with the compact body's

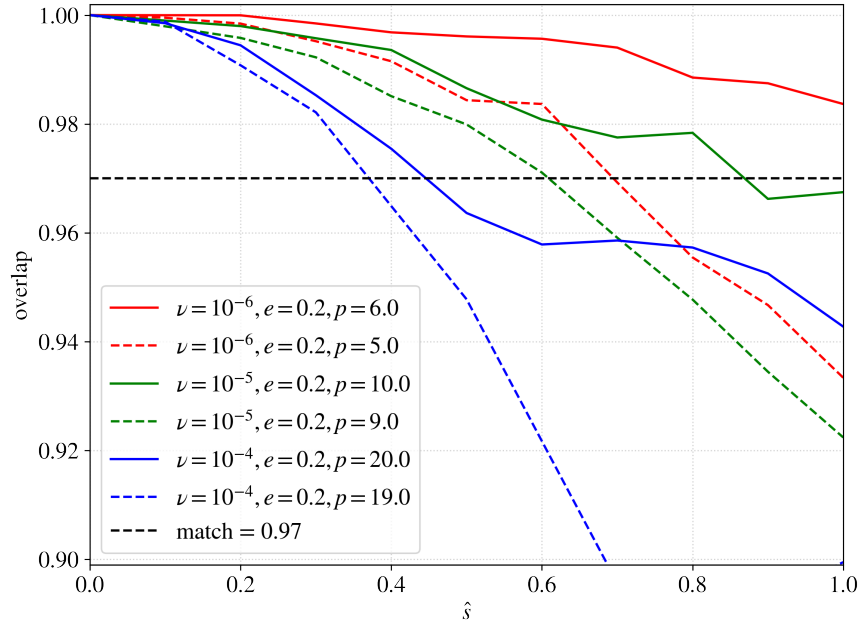


FIG. 4. Overlaps between the GW templates ($\hat{s} = 0$) and the GW signals that changed with compact body's spin \hat{s} . $M_{\text{bh}} = 10^6 M_{\odot}$, $a = 0.9$, $\iota_0 = 0.0$, $\mu_2 = 0$ and $C_Q = 0.0$. The red, green, and blue curve mark the symmetric mass ratio 10^{-6} , 10^{-5} and 10^{-4} respectively.

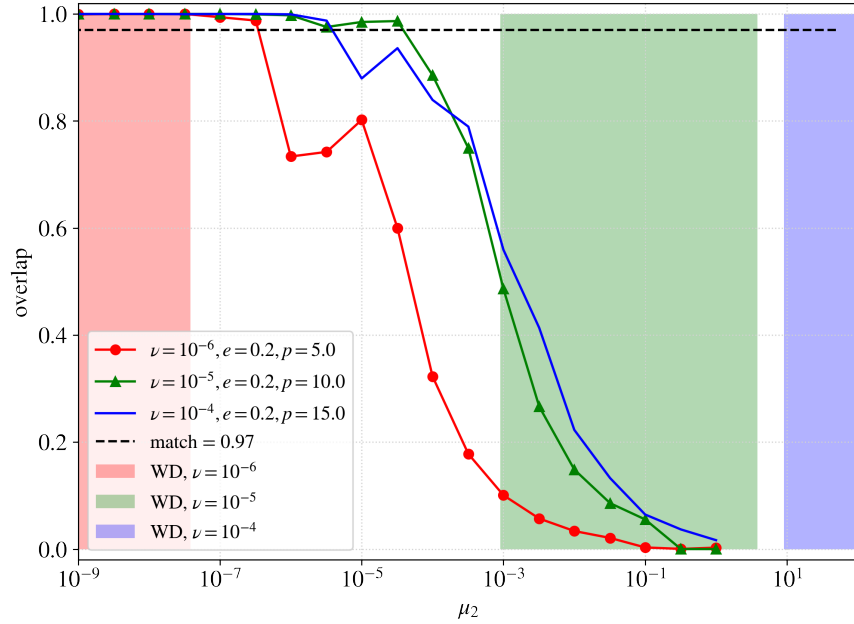


FIG. 5. Overlaps between the GW templates ($\mu_2 = 0$) and the GW signals that changed with compact body's tidal-induced quadrupole μ_2 . $M_{\text{co}} = 1 M_{\odot}$, $a = 0.9$, $\iota_0 = 0.0$, $\hat{s} = 0.0$ and $C_Q = 0.0$. The red, green, and blue curve mark the EMRIs with ν of 10^{-6} , 10^{-5} and 10^{-4} respectively. The red, green, and blue region mark the rough range of μ_2 for white dwarfs in EMRIs with different ν

spin-induced quadrupole C_Q . We can see that for most GW signals, the overlaps keep unchanged when C_Q goes up.

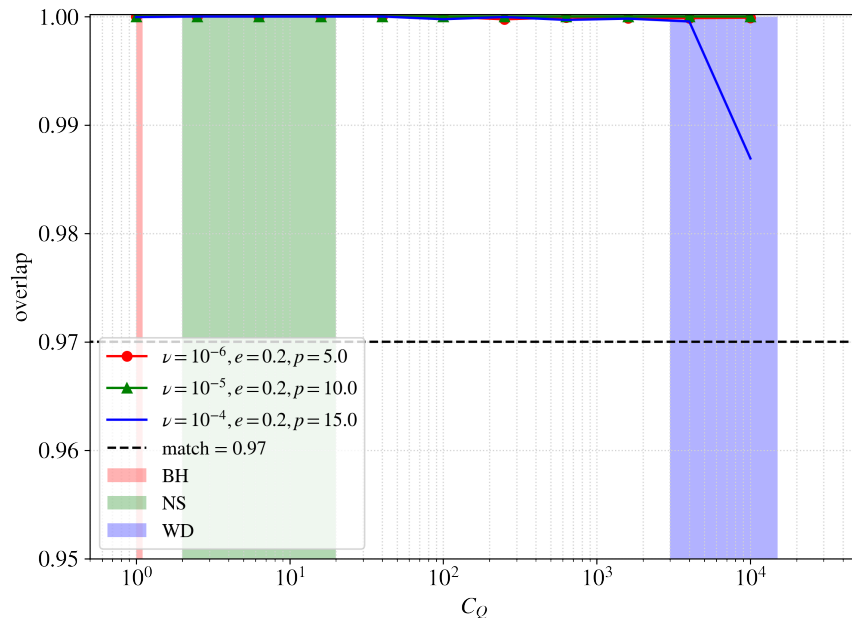


FIG. 6. Overlaps between the GW templates ($C_Q = 0$) and the GW signals that changed with compact body's spin-induced quadrupole C_Q . $M_{\text{co}} = 1 M_{\odot}$, $a = 0.9$, $\nu_0 = 0.0$, $\hat{s} = 1.0$ and $\mu_2 = 0$. The red, green, and blue curve mark the EMRIs with ν of 10^{-6} , 10^{-5} and 10^{-4} respectively. The red, green, and blue region mark the range of C_Q for black holes, neutrons stars and white dwarfs.

In the case of $\nu = 10^{-4}$, the overlaps decrease a little for $C_Q \sim 10^4$. Therefore, considering the results of Fig.5 and Fig.6, for the small body in the EMRI with $\sim 1 M_{\odot}$ mass and ν of $10^{-4} - 10^{-5}$, we could distinguish white dwarfs from other compact objects. Meanwhile, the quadrupole of black holes and neutron stars in EMRIs do not influence the GW signals.

TABLE III. Fisher Matrix Results

ν	$\Delta M_{\text{co}}/M_{\text{co}}$	$\Delta \hat{s}/\hat{s}$	$\Delta \mu_2/\mu_2$	$\Delta C_Q/C_Q$
10^{-6}	$\sim 10^{-5}$	$\sim 10^{-1}$	—	—
10^{-5}	$\sim 10^{-5}$	$\sim 10^{-1}$	$\sim 10^{-1}$	—
10^{-4}	$\sim 10^{-6}$	$\sim 10^{-2}$	$\sim 10^{-2}$	$\sim 10^{-1}$

We use the Fisher information matrix to discuss further the parameter estimation accuracy for \hat{s} , μ_2 , and C_Q . Fisher information matrix Γ is an important method for parameter analysis and estimation[48]. The matrix for a GW signal h parameterized by λ is given by

$$\Gamma_{i,j} = \left\langle \frac{\partial h}{\partial \lambda_i} \middle| \frac{\partial h}{\partial \lambda_j} \right\rangle \quad (4.4)$$

where $\lambda = (M_{\text{co}}, \hat{s}, \mu_2, C_Q)$ for EMRIs. The parameter estimation errors $\Delta \lambda$ due to Gaussian noise have the normal distribution $\mathcal{N}(0, \Gamma^{-1})$ in the case of high SNR, and the root-mean-square errors in the general case can be approximated as

$$\Delta \lambda_i = \sqrt{(\Gamma^{-1})_{i,i}} \quad (4.5)$$

We calculate the relative errors ($\Delta \lambda/\lambda$) for M_{co} , \hat{s} , μ_2 and C_Q , and the luminosity distance of GW signals is set to 1 Gpc. As shown in Table. III, the accuracy of parameter estimation gets better as ν increase. For the $\nu = 10^{-6}$ case, $\Delta M_{\text{co}}/M_{\text{co}}$ reaches the accuracy of $\sim 10^{-5}$, which shows EMRI's potential for GW detection, $\Delta \hat{s}/\hat{s}$ reaches the accuracy of $\sim 10^{-1}$, and we can not get valid results of $\Delta \mu_2/\mu_2$ and $\Delta C_Q/C_Q$. For the $\nu = 10^{-5}$ case, $\Delta M_{\text{co}}/M_{\text{co}}$

reaches the accuracy of $\sim 10^{-5}$, $\Delta\hat{s}/\hat{s}$ reaches the accuracy of $\sim 10^{-1}$, and $\Delta\mu_2/\mu_2$ reaches the accuracy of $\sim 10^{-1}$. For the $\nu = 10^{-4}$ case, $\Delta M_{\text{co}}/M_{\text{co}}$ reaches the accuracy $\sim 10^{-6}$, $\Delta\hat{s}/\hat{s}$ reaches the accuracy of $\sim 10^{-2}$, $\Delta\mu_2/\mu_2$ reaches the accuracy of $\sim 10^{-2}$, and $\Delta C_Q/C_Q$ reaches the accuracy of $\sim 10^{-1}$.

V. CONCLUSION

In this article, we use the MPD equation to simulate the GW signals of EMRIs. In this case, the small body in the EMRI is an extended body rather than a test particle. We study the influence of the small body's spin and quadrupole on the GW signals and discuss the possibility of revealing the small-body structure from the GW data.

Using the Fisher information matrix, we present the accuracy of parameter estimation for the EMRI. We find that the small body's mass could be determined accurately, and the relative error is around $\sim 10^{-5} - 10^{-6}$, which shows the potential of the EMRI in GW detection. The relative error of the small body's spin could be determined at $10^{-1} - 10^{-2}$ for different ν of EMRIs, which means spin plays an essential role in the waveform of EMRIs. However, the spin-induced and tidal-induced quadrupoles only matter for white dwarfs in EMRIs of higher symmetric mass ratio, and could be determined at $10^{-1} - 10^{-2}$. Therefore, we can distinguish the white dwarfs from other compact objects by the GW signals of EMRIs. There are no detectable effects on GW signals for the quadrupole of black holes and neutron stars in EMRIs. Meanwhile, when considering the above coefficient (\hat{s} , C_q , and μ_2 of the small body), the SNRs of the GW signals do not change much, and we can neglect the spin and quadrupole of the compact object in the waveform templates of EMRIs.

ACKNOWLEDGEMENTS

This work was supported by NSFC(National Natural Science Foundation of China) no. 11773059, the Key Research Program of Frontier Sciences, CAS(Chinese Academy of Sciences), no. QYZDB-SSW-SYS016, MEXT(Ministry of Education, Culture, Sports, Science and Technology - Japan), JSPS(The Japan Society for the Promotion of Science) Leading-edge Research Infrastructure Program, JSPS Grant-in-Aid for Specially Promoted Research 26000005, JSPS Grant-in-Aid for Scientific Research on Innovative Areas 2905: JP17H06358, JP17H06361, and JP17H06364, JSPS Core-to-Core Program A. Advanced Research Networks, JSPS Grant-in-Aid for Scientific Research (S) 17H06133, the joint research program of the Institute for cosmic Ray Research, University of Tokyo, the LIGO(The Laser Interferometer Gravitational-Wave Observatory) project, and the Virgo project. This work made use of the High Performance Computing Resource in the Core Facility for Advanced Research Computing at Shanghai Astronomical Observatory. We also thank Dr. Carlos A. Benavides-Gallego for his valuable advice on this work.

-
- [1] B.P. Abbott *et al.* (The LIGO Scientific Collaboration and the Virgo Collaboration), "Observation of gravitational waves from a binary black hole merger," *Phys. Rev. Lett.* **116**, 061102 (2016).
 - [2] B.P. Abbott *et al.* (The LIGO Scientific Collaboration and the Virgo Collaboration), "GW170817: observation of gravitational waves from a binary neutron star inspiral," *Phys. Rev. Lett.* **119**, 161101 (2017).
 - [3] Pau Amaro-Seoane, Jonathan R Gair, Marc Freitag, M Coleman Miller, Ilya Mandel, Curt J Cutler, and Stanislav Babak, "Intermediate and extreme mass-ratio inspirals—astrophysics, science applications and detection using lisa," *Classical and Quantum Gravity* **24**, R113 (2007).
 - [4] Jonathan R Gair, Christopher Tang, and Marta Volonteri, "Lisa extreme-mass-ratio inspiral events as probes of the black hole mass function," *Phys. Rev. D* **81**, 104014 (2010).
 - [5] F. Tisserand, *Traité de mécanique céleste*, Vol. 1 (Gauthier-Villars, Paris, 1889).
 - [6] Robert M Wald, "Introduction to gravitational self-force," arXiv e-prints (2009), arXiv:0907.0412.
 - [7] M Mathisson, "Neue mechanik materieller systeme," *Acta Phys. Pol.* **6**, 163 (1937).
 - [8] Achille Papapetrou, "Spinning test-particles in general relativity. i," *Proc. R. Soc. A* **209**, 248–258 (1951).
 - [9] H Hönll and A Papapetrou, "Über die innere bewegung des elektrons. iii," *Z. Phys.* **116**, 153–183 (1940).
 - [10] Ernesto Corinaldesi and Achille Papapetrou, "Spinning test-particles in general relativity. ii," *Proc. R. Soc. A* **209**, 259–268 (1951).
 - [11] W Tulczyjew, "Motion of multipole particles in general relativity theory," *Acta Phys. Pol* **18**, 393 (1959).
 - [12] B Tulczyjew and W Tulczyjew, *Recent Developments in General Relativity* (Pergamon Press, New York, 1962).
 - [13] Christian Møller, *On the definition of the centre of gravity of an arbitrary closed system in the theory of relativity* (Dublin Institute for Advanced Studies, Dublin, 1949).
 - [14] W Beiglböck, "The center-of-mass in einsteins theory of gravitation," *Commun. Math. Phys.* **5**, 106–130 (1967).

- [15] William G Dixon, “A covariant multipole formalism for extended test bodies in general relativity,” *Nuovo Cim.* **34**, 317–339 (1964).
- [16] William G Dixon, “Dynamics of extended bodies in general relativity. i. momentum and angular momentum,” *Proc. R. Soc. A* **314**, 499–527 (1970).
- [17] William G Dixon, “The definition of multipole moments for extended bodies,” *Gen. Relativ. Gravit* **4**, 199–209 (1973).
- [18] Jürgen Ehlers and Ekkart Rudolph, “Dynamics of extended bodies in general relativity center-of-mass description and quasirigidity,” *Gen. Relativ. Gravit* **8**, 197–217 (1977).
- [19] Dinesh Singh, “The mpd equations in analytic perturbative form,” *Fund. Theor. Phys.* **179**, 191–213 (2015).
- [20] Robert Wald, “Gravitational spin interaction,” *Phys. Rev. D* **6**, 406 (1972).
- [21] KP Tod, F De Felice, and M Calvani, “Spinning test particles in the field of a black hole,” *Nuovo Cim. B* **34**, 365–379 (1976).
- [22] O Semerák, “Spinning test particles in a kerr field—i,” *Mon. Not. R. Astron. Soc.* **308**, 863–875 (1999).
- [23] Shingo Suzuki and Kei-ichi Maeda, “Innermost stable circular orbit of a spinning particle in kerr spacetime,” *Phys. Rev. D* **58**, 023005 (1998).
- [24] Shingo Suzuki and Kei-ichi Maeda, “Signature of chaos in gravitational waves from a spinning particle,” *Phys. Rev. D* **61**, 024005 (1999).
- [25] Michael D Hartl, “Dynamics of spinning test particles in kerr spacetime,” *Phys. Rev. D* **67**, 024005 (2003).
- [26] Michael D Hartl, “Survey of spinning test particle orbits in kerr spacetime,” *Phys. Rev. D* **67**, 104023 (2003).
- [27] Yasushi Mino, Masaru Shibata, and Takahiro Tanaka, “Gravitational waves induced by a spinning particle falling into a rotating black hole,” *Phys. Rev. D* **53**, 622 (1996).
- [28] Craig W Lincoln and Clifford M Will, “Coalescing binary systems of compact objects to (post) 5/2-newtonian order: Late-time evolution and gravitational-radiation emission,” *Phys. Rev. D* **42**, 1123 (1990).
- [29] Wen-Biao Han and Ran Cheng, “Dynamics of extended bodies with spin-induced quadrupole in kerr spacetime: generic orbits,” *Gen. Relativ. Gravit* **49**, 48 (2017).
- [30] Jan Steinhoff and Dirk Puetzfeld, “Influence of internal structure on the motion of test bodies in extreme mass ratio situations,” *Phys. Rev. D* **86**, 044033 (2012).
- [31] William G Laarakkers and Eric Poisson, “Quadrupole moments of rotating neutron stars,” *Astrophys. J* **512**, 282 (1999).
- [32] Nami Uchikata, Shijun Yoshida, and Paolo Pani, “Tidal deformability and i-love-q relations for gravastars with polytropic thin shells,” *Phys. Rev. D* **94**, 064015 (2016).
- [33] Tatsuya Narikawa, Nami Uchikata, and Takahiro Tanaka, “Gravitational-wave constraints on the gwtc-2 events by measuring the tidal deformability and the spin-induced quadrupole moment,” *Phys. Rev. D* **104**, 084056 (2021).
- [34] Muhammed Saleem, NV Krishnendu, Abhirup Ghosh, Anuradha Gupta, W Del Pozzo, Archisman Ghosh, and KG Arun, “Population inference of spin-induced quadrupole moments as a probe for nonblack hole compact binaries,” *Phys. Rev. D* **105**, 104066 (2022).
- [35] Kuantay Boshkayev, Jorge A Rueda, Remo Ruffini, and Ivan Siutsou, “On general relativistic uniformly rotating white dwarfs,” *Astrophys. J* **762**, 117 (2012).
- [36] Taylor Binnington and Eric Poisson, “Relativistic theory of tidal love numbers,” *Phys. Rev. D* **80**, 084018 (2009).
- [37] Andrew J Taylor, Kent Yagi, and Phil L Arras, “I-love-q relations for realistic white dwarfs,” *Monthly Notices of the Royal Astronomical Society* **492**, 978–992 (2020).
- [38] Misao Sasaki, Teruaki Suyama, Takahiro Tanaka, and Shuichiro Yokoyama, “Primordial black hole scenario for the gravitational-wave event gw150914,” *Phys. Rev. Lett.* **117**, 061101 (2016).
- [39] Michele Maggiore, *Gravitational Waves: Volume 2: Astrophysics and Cosmology* (Oxford University Press, 2018).
- [40] James M Bardeen, William H Press, and Saul A Teukolsky, “Rotating black holes: locally nonrotating frames, energy extraction, and scalar synchrotron radiation,” *Astrophys. J* **178**, 347–370 (1972).
- [41] Kostas Glampedakis, Scott A Hughes, and Daniel Kennefick, “Approximating the inspiral of test bodies into kerr black holes,” *Phys. Rev. D* **66**, 064005 (2002).
- [42] Jonathan R Gair and Kostas Glampedakis, “Improved approximate inspirals of test bodies into kerr black holes,” *Phys. Rev. D* **73**, 064037 (2006).
- [43] Shuo Xin, Wen-Biao Han, and Shu-Cheng Yang, “Gravitational waves from extreme-mass-ratio inspirals using general parametrized metrics,” *Phys. Rev. D* **100**, 084055 (2019).
- [44] Stanislav Babak, Hua Fang, Jonathan R Gair, Kostas Glampedakis, and Scott A Hughes, ““kludge” gravitational waveforms for a test-body orbiting a kerr black hole,” *Phys. Rev. D* **75**, 024005 (2007).
- [45] Lee S Finn, “Detection, measurement, and gravitational radiation,” *Phys. Rev. D* **46**, 5236 (1992).
- [46] Alex Nitz, Ian Harry, Duncan Brown, Christopher M. Biwer, Josh Willis, Tito Dal Canton, Collin Capano, Larne Pekowsky, Thomas Dent, Andrew R. Williamson, Soumi De, Miriam Cabero, Bernd Machenschalk, Duncan Macleod, Prayush Kumar, Steven Reyes, Thomas Massinger, Gareth Davies, Marton Tapai, dfinstad, Stephen Fairhurst, Sebastian Khan, Alex Nielsen, shasvath, Francesco Panarale, Leo Singer, Hunter Gabbard, idorington92, Lorena Magana Zertuche, and Bhooshan Uday Varsha Gadre, “gwastro/pycbc: Pycbc release v1.14.0,” (2019).
- [47] Nicolas Yunes, Alessandra Buonanno, Scott A Hughes, Yi Pan, Enrico Barausse, M Coleman Miller, and William Throwe, “Extreme mass-ratio inspirals in the effective-one-body approach: Quasicircular, equatorial orbits around a spinning black hole,” *Phys. Rev. D* **83**, 044044 (2011).
- [48] Curt Cutler and Eanna E Flanagan, “Gravitational waves from merging compact binaries: How accurately can one extract the binary’s parameters from the inspiral waveform?” *Phys. Rev. D* **49**, 2658 (1994).